

On the monitoring and early-warning of brittle slope failures in hard rock masses: Examples from an open-pit mine



Tommaso Carlà^{a,b,*}, Paolo Farina^b, Emanuele Intrieri^b, Kostas Botsialas^c, Nicola Casagli^b

^a Regional Doctoral School of Earth Sciences, Università degli Studi di Firenze, Via La Pira 4, 50121 Firenze, Italy

^b Department of Earth Sciences, Università degli Studi di Firenze, Via La Pira 4, 50121 Firenze, Italy

^c Geotechnical Engineer of the open-pit mine, Norway

ARTICLE INFO

Keywords:

Brittle failure
Slope monitoring
Ground-based radar
Open-pit mine
Tertiary creep

ABSTRACT

The management of unstable slopes is one of the most critical issues when dealing with safety in open-pit mines. Suitable notice of impending failure events must be provided, and at the same time the number of false alarms must be kept to a minimum to avoid financial losses deriving from unnecessary outages of the production works. Comprehensive slope monitoring programs and early warning systems are usually implemented to this aim. However, systematic procedures for their tuning are lacking and several key factors are often overlooked. Therefore the mitigation of slope failure risk is still a topic of great concern, especially in open-pit mines excavated through hard rock masses featuring markedly brittle behavior, which supposedly provide little or no measurable precursors to failure. In this paper, 9 instabilities occurred at an undisclosed open-pit mine, and monitored by ground-based radar devices, were reviewed with the goal of characterizing the typical slope deformation behavior and defining the appropriate strategy for the setup of alarms. The estimated mass of the case studies ranged from 1500 t to 750,000 t. 5 instabilities culminated to failure, whereas the other 4, although showing considerable amounts and rates of movement, ultimately did not fail. The analysis provided critical insights into the deformation of hard rock masses of high geomechanical quality, and allowed the identification of “signature” parameters of the failure events. General operative recommendations for effective slope monitoring and early warning were consequently derived.

1. Introduction

Detecting ongoing processes of rock slope deformation that may lead to failure is a critical aspect in the fields of geomechanics and engineering geology. Mitigation of slope failure risk requires knowledge of the structural geology, of the rock mass properties, and of the influence of water and other external forces in the monitored area. The topic is of particular concern in open-pit mines, where production works must proceed at high rate, and at the same time the safety of the personnel and the integrity of the mining equipment must be guaranteed.

Regardless of the driving factors, displacement and velocity are widely considered as the best indicators of slope stability conditions (Lacasse and Nadim, 2009; Intrieri et al., 2013). Several time-dependent relationships have been proposed to fit monitoring data of slopes approaching failure (Federico et al., 2012; Intrieri and Gigli, 2016). Most of these are based on the observation that slope velocity increases asymptotically towards failure (“tertiary” or “accelerating” creep, usually known as “progressive deformation” in the mining field), and

are solved with the application of the inverse velocity method developed by Fukuzono (1985), (Voight, 1988; 1989). Accordingly, monitoring ground surface movements is one of the fundamental precautionary measures of open-pit mine operations, and a variety of instruments may be used to this aim (Read and Stacey, 2009; Vaziri et al., 2010). In particular, ground-based radar has become one of the leading-edge technologies, due to its ability to detect movements with high accuracy, spatial coverage and frequency of acquisition. Several successful applications of ground-based radar systems to identify large-scale failures in open-pit mines have been published in the literature (Armstrong and Rose, 2009; Doyle and Reese, 2011; Ginting et al., 2011; Farina et al., 2013; Macqueen et al., 2013; Farina et al., 2014; Atzeni et al., 2015; Dick et al., 2015).

Even though tertiary creep may be assumed as a precondition for failure occurrence, prediction and early warning are still difficult to obtain because of the variability of slope behaviors. Phases of progressive deformation may in fact develop rapidly or over very long periods of time, involve a wide range of possible rates, and show an alternation of acceleration-deceleration cycles (Zavodni and Broadbent,

* Corresponding author at: Regional Doctoral School of Earth Sciences, Università degli Studi di Firenze, Via La Pira 4, 50121 Firenze, Italy.
E-mail address: tommaso.carla@unifi.it (T. Carlà).

1980; Hutchinson, 2001; Crosta and Agliardi, 2002). While large-scale failures that are anticipated by extended periods of progressive deformation (i.e. ductile behavior) are relatively easy to predict, in other geological conditions failures can be brittle (even though brittleness is properly referred to a post-failure behavior consisting in an abrupt strength drop, here it is used to indicate failures characterized by little or negligible precursor deformation) (Eberhardt et al., 2004; Rose and Hungr, 2007; Paronuzzi et al., 2016). Markedly brittle failures in tension or shear on steep slopes, especially if related to small-scale slides and hard rock masses (e.g. high-grade metamorphic or volcanic rocks), usually are the most difficult to predict. Anticipated by seemingly step-like, nearly instantaneous displacements, it is common perception that these cannot be identified with sufficient advance (Rose and Hungr, 2007).

In this paper we present 9 cases of slope instability monitored by means of ground-based radar devices at an undisclosed open-pit mine. The pit is excavated through an ore body consisting of hard rock formations of high mechanical quality in terms of Rock Mass Rating (RMR). 5 of these movements reached failure, whereas the other 4, although showing intense phases of deformation, ultimately did not (“non-failures” in the rest of the paper). With the goal of supporting the tuning of an ad-hoc early warning system, the analysis of the monitoring data provided new insights into the precursory deformation in markedly brittle rock slope failures. Thanks to the high temporal resolution of ground-based radar data, it was observed that the pit slopes are subject to very rapid phases of tertiary creep, and that “signature” parameters differently described failures and non-failures. General operative recommendations for effective slope monitoring and early warning were consequently derived. Finally, methodologies to be used for the activation of alarms at the pit were defined.

2. Overview of the open-pit and of the instability case studies

Name and location of the open-pit operation object of the present study are confidential and therefore cannot be disclosed, as well as specific details concerning the mined ore body. The mine (which has been active for over 50 years) has a length of roughly 3 km, a width between 400 m and 600 m, and a current depth > 200 m (Fig. 1). Benches are either 15 or 30 m high (depending on the stage of production), and the overall slope angle of the pit is between 45° and 55°. According to the RMR classification, the rock mass quality in the pit mostly ranges between “fair” and “very good”, with values that on average are included between 60 and 80 (thus falling in the “good” category). Instabilities are typically structurally controlled and relatively shallow. These include planar, wedge and toppling mechanisms, while there are no records of identified deep-seated movements. Extremely large-scale movements are also uncommon. The highest risk is posed by rockfall and by single or multiple bench scale failures of small to medium size. Specifically, the mass of the instabilities discussed in this paper ranges from 1000 to 750,000 t.

2.1. Geological and structural setting

From a geological point of view, the ore body consists of an intrusion through an enclosing anorthosite formation. Xenoliths of anorthosite are also present within the ore, along with two major cross-cutting diabase dikes of sub-vertical inclination. Both the ore body and the enclosing anorthosite are characterized by several areas of heavy alteration related to fractures and fault systems. In correspondence of their contact, movement indicators like S–C fabrics, secondary structures, and slickensides can be observed.

In the area of the pit 6 different joint sets, distributed in 8 different geological domains, were defined (Morales et al., 2017). The structural fabric derived by these domains leads to the formulation of wedges/tetrahedrals, which may be unstable when the required kinematic conditions are fulfilled. As a result planar, wedge, and toppling

instabilities have taken place during the operational life of the mine. The geometrical relationship between slope faces and fracture planes, and the deterioration of the mechanical properties of the planes, are the main predisposing factors. In some cases, even if the kinematic conditions for the initiation of an instability were reached, the wedges prone to slide did not show any displacement for many years. Discontinuities are occasionally filled with clayey material, and free swell of up to 230% has been measured in some smectites. The joint wall compressive strength varies from 25 MPa to 100 MPa, depending on the degree of weathering and on the presence and type of clayey minerals. The residual friction angle can reach values as low as 24°, while the Joint Roughness Coefficient (JRC) can be of 4–6 or even lower.

2.2. Slope monitoring data

Nowadays, the use of ground-based radar in open-pit mines is a standard practice for active slope monitoring. Displacements are calculated by measuring the phase difference of the back-scattered microwave signal between two or more coherent acquisitions (Antonello et al., 2004; Luzi et al., 2006; Casagli et al., 2010; Di Traglia et al., 2014; Monserrat et al., 2014; Bardi et al., 2017; Casagli et al., 2017). The technology presents the advantages of high measurement accuracy, high spatial and temporal resolution, long-range capabilities, and limited impact of atmospheric noise (Farina et al., 2013). This is obtained without the need to install artificial reflectors on the slope.

The analyzed set of monitoring data is made of radar displacement time series from 5 cases of failure and from 4 cases of significant slope movements that did not evolve into failure. In every instance, a displacement time series was extracted by averaging data of all the pixels included in the unstable section of a single bench; meaning that one displacement time series was obtained for single bench instabilities (or smaller), whereas for multiple bench instabilities their number is equal to how many benches were involved in the detected movement. Pixel selection was based on a velocity cutoff that was in place at the mine as part of the safety strategies for slope failure risk reduction. Although measurement error varied with the level of disturbance induced by vibrations and blasting, this was generally below 0.5 mm/h. The distance between radar and monitored instability ranged from 200 m to 850 m (Fig. 1).

Depending on the radar model in use (two Real Aperture Radar and one Synthetic Aperture Radar were in operation at the mine), the frequency of acquisition was either 20 or 3 min. When dealing with high-frequency radar measurements, filtering is needed in order to remove noise and highlight the fundamental trends in the data (Dick et al., 2015; Macciotta et al., 2016; Carlà et al., 2016). Given the abrupt nature of the accelerations potentially affecting slopes in the pit, the interval over which smoothing must be performed is necessarily short, so that the detection of sudden trend changes is not crucially delayed. In this context, a better understanding of the main trends may be simply gained by reducing the number of plotted data points, grouping measurements relatively to the selected reference time window (e.g. by averaging all data acquired on the same hour, obtaining one representative value for every hour of monitoring). The analysis of the radar measurements was herein performed by considering thus calculated 1-h averaged data (Sections 3.1 and 3.3), with the exception of failure #5; a separate sub-section was dedicated to this case study due to its peculiar deformation behavior with respect to the other failures (Section 3.2).

Displacements measured by radar are relative to the direction between the target and the receiver (i.e. line-of-sight, or LOS), and therefore may not represent the full component of the actual movement. The latter aspect is often not taken in due consideration, which potentially leads either to the setup of too conservative thresholds owing to uncertainty (i.e. monitoring is affected by an excessive number of false alarms, resulting in a lack of credibility to the eyes of the production team) or, even worse, to a false sense of safety.

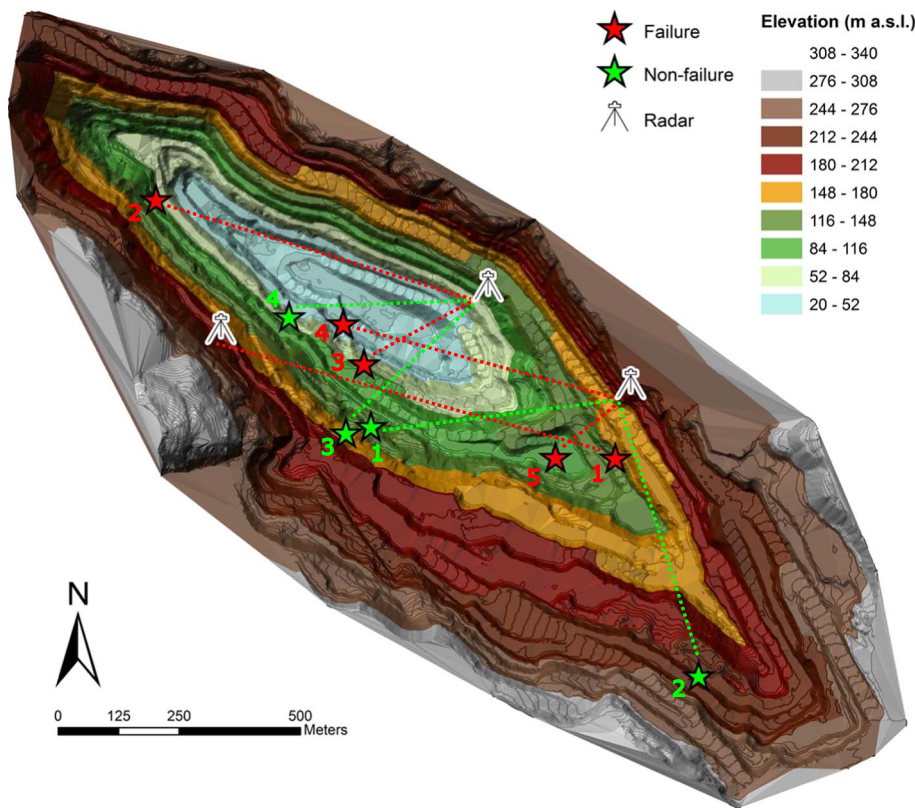


Fig. 1. Overview of the open-pit, with location of the instabilities and of the radar devices (see Table 1 for numbering of the instabilities).

Table 1

Radar LOS sensitivity to the movements of the 9 cases of slope instability in the dataset. Data of non-failures #3 and #4 are relative to bench 155 and bench 070, respectively. d = total displacement during the most significant phase of slope deformation (based on raw data, see Figs. 2–4); v_p = peak velocity (based on 1-h averaged data, see Section 3).

Case	Type	LOS sensitivity	LOS d (mm)	Actual d (mm)	LOS v_p (mm/h)	Actual v_p (mm/h)
#1	Failure	0.33	8.3	25	10	30.2
#2	Failure	0.2	13.2	66	7.4	36.8
#3	Failure	0.1	16.6	165.7	7.7	77.5
#4	Failure	0.06	12.6	210.6	3.6	60.7
#5	Failure	0.85	57.4	67.5	3.1	3.7
#1	Non-failure	0.23	53.7	233.3	2.3	10
#2	Non-failure	0.84	81.9	97.5	1.9	2.3
#3	Non-failure	0.83	393.6	474.2	21	25.3
#4	Non-failure	0.86	44.1	51.3	1.6	1.9

Concerning the presented case study, the width and depth of the pit cause the radar LOS sensitivity to be extremely variable (Fig. 1). Since the azimuth and dip direction of movement of each instability were provided by the mine technical staff, it was possible to correct all measurements to the respective actual values of displacement (Table 1). This was accomplished by considering the problem in terms of the directional cosines of the LOS versor and of the slope movement versor. The LOS sensitivity is defined using the cosine of the angle θ between these two versors, which can vary between 0 and 1. When $\text{Cos } \theta = 0$, the direction of slope movement is perpendicular to the LOS and therefore is not detectable by the radar, whereas when $\text{Cos } \theta = 1$ the direction of slope movement is parallel to the LOS and the radar sensitivity is 100% with respect to the actual values of displacement.

In order to make the monitoring data relative to the 9 case studies comparable between each other, only actual values of displacement, velocity and acceleration, corrected according to the radar LOS sensitivity, were considered. Table 1 highlights the importance of this procedure: reviewing uncorrected data would have determined a false

perception of the magnitude of the slope movements and would have most likely brought to misleading interpretations when characterizing the precursors to failure.

3. Analysis of the case studies

Four of the failures were preceded by a sudden and very rapid increment of displacement (red shaded areas in Fig. 2). Occasionally this last phase of acceleration occurred after a previous rapid increment of displacement and a very short interval of stability (cases #2 and #4 in Fig. 2b and d). In any case the greatest part of the total displacement was concentrated in a period ranging from minutes to hours before the time of failure. The pre-event deformation of the fifth failure was somewhat different (red shaded area in Fig. 3), as it developed over ~5 days and with an apparent alternation of several acceleration-deceleration cycles.

Fig. 4 details the movements of the four non-failures: total displacements were roughly of the same order of magnitude of those in Fig. 2, and in some cases were noticeably higher (cases #1 and #3 in Fig. 4a and c). Phases of intense deformation were recorded, spanning at varying rates over longer periods of time (i.e. from days to months). Moreover, rapid accelerations were observed as well, even if not leading to failure.

In the following sections, specific properties of each instability, and the analysis of the relative monitoring data, are presented to characterize the slope movements in the pit. In Fig. 5, photos of two failures and of two non-failures are shown.

3.1. Failures #1–#4

Table 2 summarizes the main characteristics of the first four failure case studies. These were all of relatively small size, involving a single rock block over a single discontinuity (or pair of discontinuities in the case of wedge mechanism) at bench or sub-bench scale (i.e. ~15 m in slope height or less). In every instance the controlling discontinuities

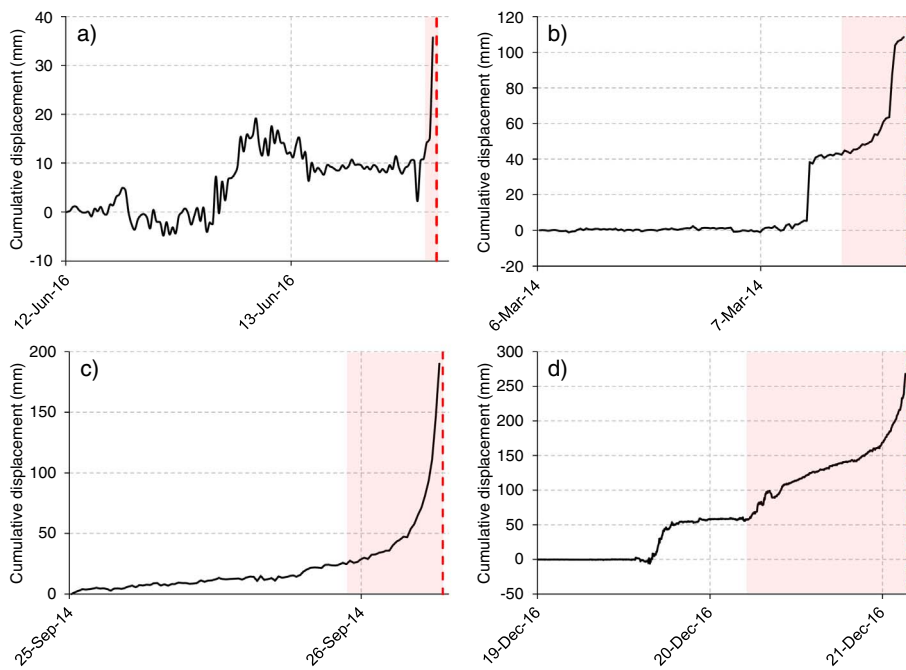


Fig. 2. Raw displacement time series of failures (a) #1, (b) #2, (c) #3, and (d) #4. The red dashed lines mark the failure-time of each event, while the red shaded areas highlight the final increment of displacement leading to failure. (For interpretation of the references to color in this figure legend, the reader is referred to the web version of this article.)

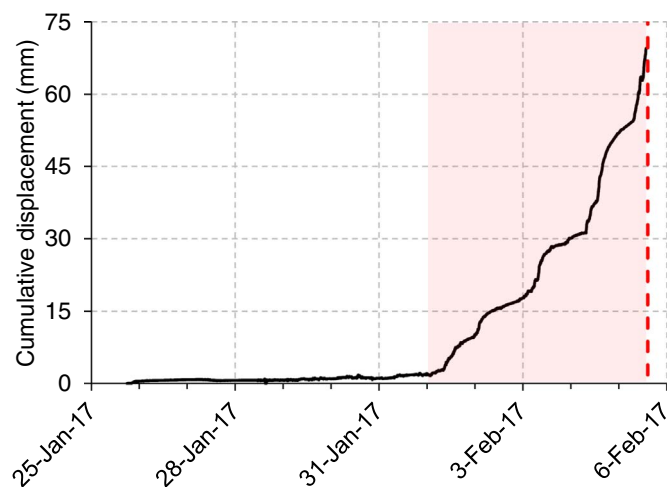


Fig. 3. Raw displacement time series of failure #5. The red dashed line marks the failure-time, while the red shaded area highlights the final increment of displacement leading to failure. (For interpretation of the references to color in this figure legend, the reader is referred to the web version of this article.)

were part of the fabric of main joint sets in the mine. The duration of the final increase of displacement leading to failure was extremely short (i.e. less than one day), and was associated with large values of velocity and acceleration. Specifically, peak velocities were recorded just before the occurrence of the failures, and ranged from 32.5 mm/h to 77.5 mm/h, while peak accelerations from 26.9 mm/h² to 44.4 mm/h².

Fig. 6 details the respective velocity plots, derived from 1-h averaged data. Especially cases #2, #3, and #4, appear to present exponential increases of slope velocity typical of tertiary creep behavior (Fig. 6b–d). At the same time the abruptness of these phases of progressive deformation, which become apparent only in the last few hours before failure, may have crucial repercussions in terms of the practical ability to successfully anticipate and predict the timing of such events in near real-time. In this sense failure #1 would be the most challenging, as a decisive increase in velocity occurred in just the last hour before the event (Fig. 6a).

Fig. 7 shows the resulting inverse velocity plots: in cases #2, #3,

and #4, the accuracy of the prediction may be considered acceptable, as the difference between the predicted and the actual time of failure is approximately one hour (the depicted time intervals cover the length of the final trends of inverse velocity towards the horizontal axis, Fig. 7b–d). The quality of the linear regression is also extremely high ($R^2 \geq 0.95$). In hindsight, it appears that in case #3 a linear fitting is not the most ideal way of extrapolating the data, as an even better prediction would probably be obtained by factoring the slight concavity of the curve in its last section (Fig. 7c). Case #1 does not provide a successful prediction, as the inverse velocity plot converges towards zero only in very close proximity to the time of failure, when a sufficient number of data points to be extrapolated are not yet available (Fig. 7a). It should be noted that the latter was one of the instabilities that was monitored with a 20-min sampling rate. A higher frequency of acquisition (e.g. 3-min sampling rate) would have arguably evidenced a smoother tertiary creep behavior.

3.2. Failure #5

While failures #1–#4 shared many similarities in terms of deformation behavior, failure #5 may be distinguished from those according to a number of different aspects. This case study was in fact a bench scale toppling (Fig. 5c) with a mass of approximately 10,000 t, which experienced a phase of precursor deformation that persisted for a longer time interval before the failure (5 days). The raw radar data relative to the unstable slope sector showed alternating accelerations and decelerations. The mine staff reported that this may have been partly due to the ongoing production works and to the presence of machineries operating at the time in the area, which made unclear the influence of induced noise on the time series. Still, it is sure that the intensity of the movement rates was significantly lower than for the other failures, with peak velocity and acceleration of only 3.7 mm/h and 1.8 mm/h² registered few instants before the failure.

Despite the irregularity of the measured displacements, progressive deformation of the slope prior to the failure may still be observed (Fig. 3). In this case 1-h averaged data are not appropriate to smooth out the alternating phases of acceleration and deceleration (Fig. 8a), and a longer-term smoothing is needed for the purposes of failure-time prediction; in retrospect, 1-day averaged data (i.e. obtained by averaging all measurements that were acquired on the same day) were thus

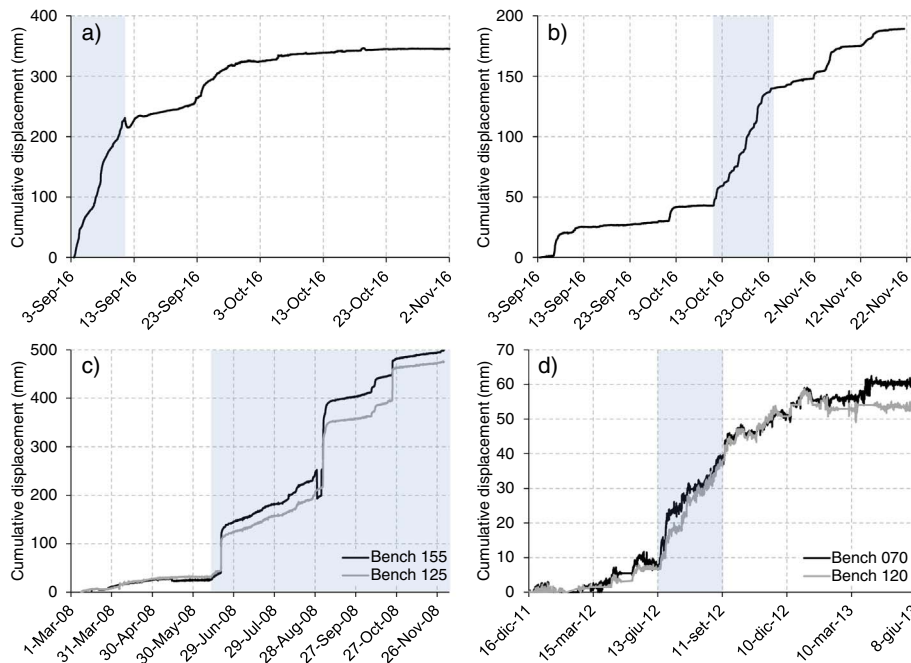


Fig. 4. Displacement time series of non-failures (a) #1, (b) #2, (c) #3, and (d) #4. The blue shaded areas highlight phases of significant increment of displacement. (For interpretation of the references to color in this figure legend, the reader is referred to the web version of this article.)

also considered (Fig. 8b). As a result, the inverse velocity plot based on 1-h averaged data does not converge decisively towards the horizontal axis (Fig. 8c), whereas a more acceptable prediction may be derived by using 1-day averaged data (Fig. 8d).

3.3. Non-failures

Table 3 describes the main characteristics of the non-failure case studies. These instabilities experienced prolonged and intense periods of deformation (lasting from several days to several months) and, with the exception of the case #2 toppling, also involved significantly larger volumes of rock with respect to the cases of failure (both single bench and multiple bench movements, Fig. 5b and d). Within such phases of deformation, which ultimately did not lead to failure, peak velocity and acceleration ranged from 1.9 mm/h to 25.3 mm/h and from 1.4 mm/h² to 14.9 mm/h², respectively.

Table 2

Characteristics of failures #1, #2, #3, and #4.

Case	Mechanism	Estimated mass (t)	D (hours)*	Actual v_p (mm/h)**	Actual a_p (mm/h ²)**
#1	Wedge	4000	~1.5	30.2	24.5
#2	Planar	4000	~7	36.8	29
#3	Wedge	1500	~8	77.5	44.4
#4	Wedge	3000	~22	60.7	34.3

D = Duration of the final increment of displacement leading to failure (red shaded areas in Fig. 2); * v_p = peak velocity prior to failure; ** a_p = peak acceleration prior to failure. **Derived from raw monitoring data (F 2). **Derived from 1-h averaged data (Fig. 6).

Fig. 9 details the plots of 1-h averaged velocity with time. Case #3 experienced three rapid accelerations of very similar form during the monitoring period (Fig. 4c); only the first and most intense of these

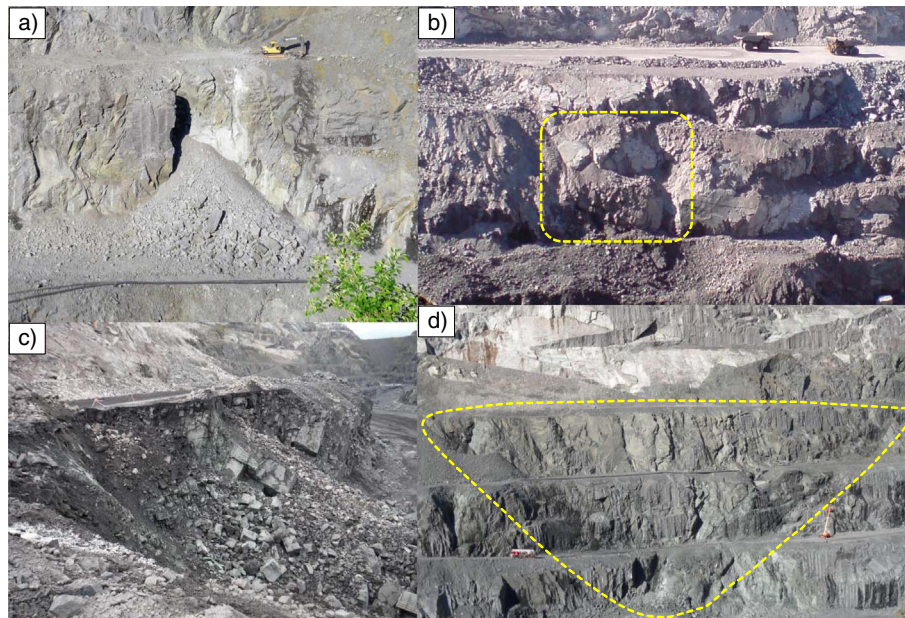


Fig. 5. Photos of (a) failure #2, (b) non-failure #1, (c) failure #5, and (d) non-failure #4. In the non-failures, the yellow dashed lines delimit the extent of the slope movement detected by the radar. (For interpretation of the references to color in this figure legend, the reader is referred to the web version of this article.)

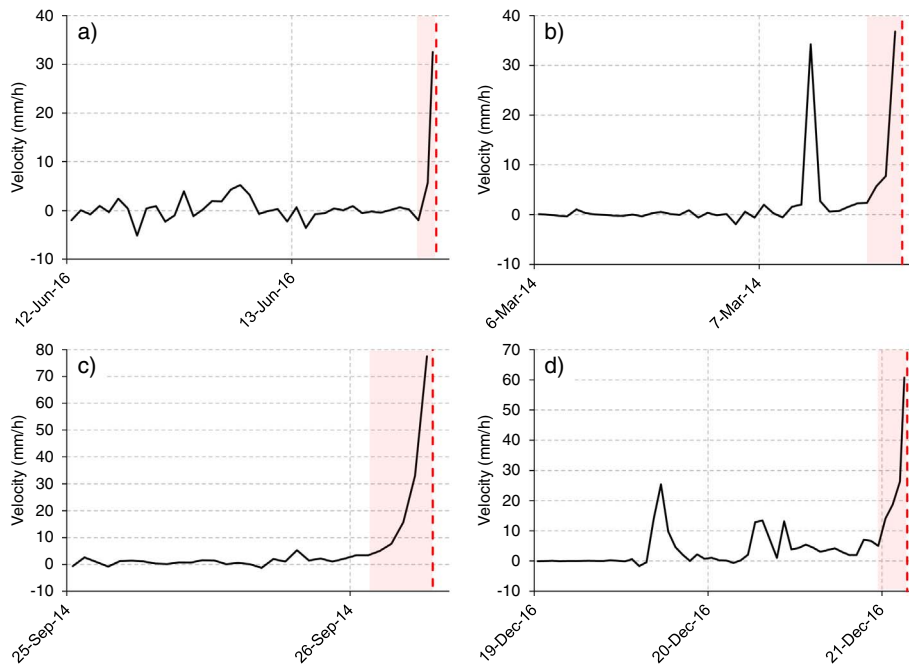


Fig. 6. Velocity plots of failures (a) #1, (b) #2, (c) #3, and (d) #4. The red dashed lines mark the failure-time of each event, while the red shaded areas highlight the final increment of velocity leading to failure. (For interpretation of the references to color in this figure legend, the reader is referred to the web version of this article.)

events is shown in Fig. 9c for illustration purposes. In the other cases, the considered time intervals are relative to the previously indicated phases of significant increment of displacement (*D* in Table 3 and blue shaded areas in Fig. 4). Concerning case #4, only data relative to bench 070 are shown, again for illustration purposes.

In the velocity plots of non-failures #1 and #3, tertiary creep may be observed on 7 September 2016 and 19 June 2008, respectively (Fig. 9a and c). Non-failures #2 and #4 instead did not show evidences of progressive deformation, as velocities appear to be irregularly scattered across values < 2.5 mm/h (Fig. 9b and d). The velocity plot of case #2 may somewhat resemble that relative to 1-h averaged data of failure #5 (Fig. 8a), with a sequence of alternating phases of acceleration and deceleration; interestingly, both instabilities were the only ones in the dataset to feature toppling mechanism. However, non-

failure #2 did not yield a clear increase of velocity with time, as detected in Fig. 8b; filtering to 1-day averaged data also produced a significantly lower peak velocity (10.7 mm/d, as opposed to 30.7 mm/d of failure #5).

Fig. 10 depicts the corresponding inverse velocity plots for the aforementioned acceleration events of non-failures #1 and #3. Both plots present a linear downward trend, which is then followed by an upward trend indicating a progressive deceleration of the slope away from a condition of failure. The red shaded areas mark the plot sections that could be considered for extrapolation of a linear regression line towards the horizontal axis and consequently for producing a failure-time prediction. Assuming a scenario of near real-time monitoring, the application of the inverse velocity approach to these cases would therefore lead to the inevitable issuing of false alarms, even more if

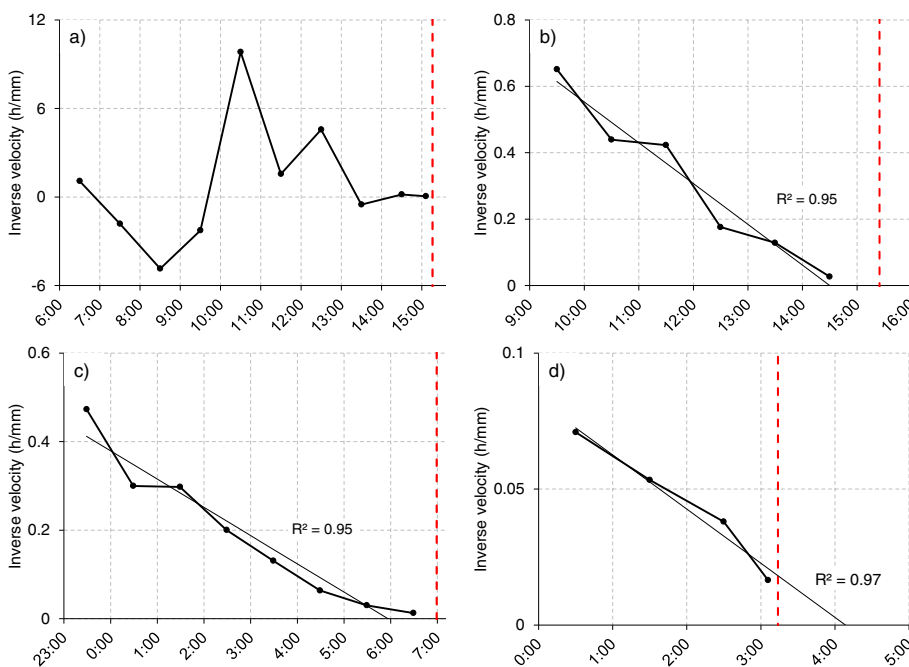


Fig. 7. Inverse velocity plots of failures (a) #1 (13 June 2016), (b) #2 (7 March 2014), (c) #3 (25–26 September 2014), and (d) #4 (21 December 2016). The red dashed lines mark the failure-time of each event. (For interpretation of the references to color in this figure legend, the reader is referred to the web version of this article.)

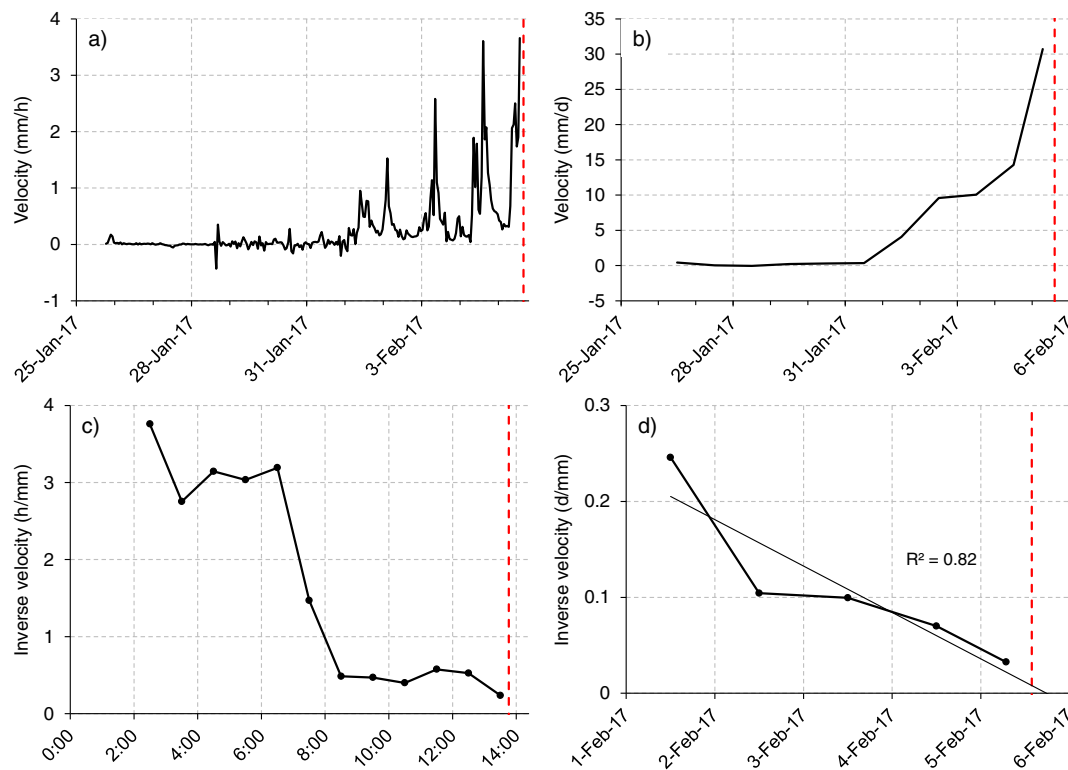


Fig. 8. Failure #5: (a) 1-h averaged velocity, (b) 1-day averaged velocity, (c) 1-h averaged inverse velocity (5 February 2017), and (d) 1-day averaged inverse velocity. The red dashed lines mark the failure-time. (For interpretation of the references to color in this figure legend, the reader is referred to the web version of this article.)

Table 3

Characteristics of non-failures #1, #2, #3, and #4.

Case	Mechanism	Estimated mass (t)	D (days)*	Actual v_p (mm/h)**	Actual a_p (mm/h ²)**
#1	Planar	35,000	9	10	7.4
#2	Toppling	7500	13	2.3	1.2
#3	Wedge	92,000	270	25.3	14.9
#4	Wedge	750,000	205	1.9	1.4

D = Duration of significant increment of displacement that did not lead to failure (blue shaded areas in Fig. 4); * v_p = peak velocity; ** a_p = peak acceleration.**

*Derived from raw monitoring data (Fig. 4). **Derived from 1-h averaged data (Fig. 9).

considering the significant rates of slope movement associated with these tertiary creep phases (peak velocities of 10 mm/h and 25.3 mm/h in non-failures #1 and #3, respectively).

4. Discussion

Several useful inputs regarding slope failure predictability, and the requisites that are necessary to implement effective monitoring programs and early warning systems, may be derived from the presented radar data. In particular, these apply to the risk mitigation in slopes that are potentially affected by rapid accelerations.

4.1. Temporal evolution of the displacements and tertiary creep

Increments of the slope displacements in the pit can be sudden and extremely rapid: in particular, failures #1–#4 were all anticipated by accelerations that lasted for only few hours (Figs. 2 and 6), while negligible amounts of deformation were measured before their respective onset. Within the context of significantly longer phases of deformation (i.e. several days to several months), brief accelerations of similar nature were occasionally associated to non-failures as well (see cases #1 and #3 in Fig. 4a and c). The toppling failure #5 experienced

a precursor deformation with a somewhat intermediate behavior between the rapid movements of failures #1–#4 and the prolonged phases of deformation of the other non-failure case studies.

Interestingly, these accelerations may be related to phases of tertiary creep. Data from failure #1, which featured the most rapid of the observed events of acceleration in the dataset (Fig. 6a), did not show clear progressive deformation arguably because of the inadequacy of the 20-min sampling rate by which this instability was monitored. The apparent lack of tertiary creep prior to brittle failure in hard rock masses, as described by Rose and Hungr (2007), is thus likely to be related to an issue of too low frequency of measurement acquisition, and not to a different slope kinematics.

4.2. LOS sensitivity

The impact of the LOS assumes pivotal importance, as an incorrect data correction may decisively alter the perception of the displacements (Table 1). By knowing the positions of the radar and of the instability, along with the actual direction of slope movement, the correction of the measurements according to the radar sensitivity is a simple procedure. However, this is much less easily obtained at the scale of an open-pit mine, where instabilities may be numerous and have widely different characteristics; in addition to this point, the geometry and aspect of the rock faces frequently change in consequence of the continuous excavation works. The above applies even more to the monitoring of hard rock masses, where failures may develop very rapidly and thus give little time to assess mechanism and kinematics of movement. Given that instabilities in such a context are typically structurally controlled, the ideal solution would be to use a map of the expected direction of movement of all the sectors of the pit covered by the radar (e.g. by means of a 3D kinematic analysis Gokceoglu et al., 2000; Gigli et al., 2012; Fanti et al., 2013; Gigli et al., 2014), to calculate the sensitivity of the radar LOS to those directions, and then to define alarm thresholds based on monitoring data corrected according to the LOS sensitivity.

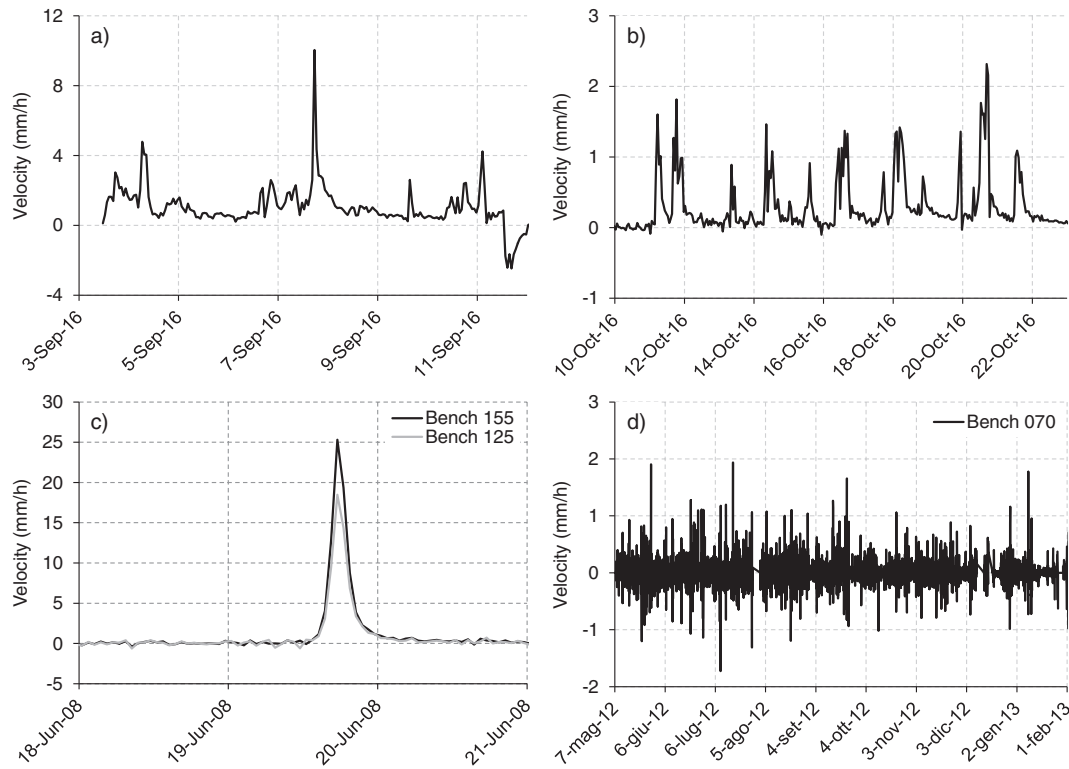


Fig. 9. Velocity plots of non-failures (a) #1, (b) #2, (c) #3, and (d) #4.

4.3. Mechanism

With regards to the mechanism of the instabilities, planar and wedge modes did not show obvious reciprocal differences in terms of trends of displacement. Conversely, a peculiar behavior was observed for the two toppling instabilities in the dataset (the effects of noise induced by the ongoing production works on the displacement measurements of failure #5 were unclear; however, given the evident similarities with data of non-failure #2, it is inferred that these were not significant). In both instances the main phase of slope deformation saw in fact the occurrence of lower rates of displacement, and of an alternation of accelerations and decelerations (Figs. 8a and 9b). This may be explained as follows: while planar and wedge instabilities involve relative movement between rock blocks with respect to one or more discontinuities, on the other hand a toppling mechanism implies the opening of a controlling sub-vertical fracture, and therefore the cyclical increase and decrease of velocity may reflect this process as it develops intermittently with time. In both cases of toppling, the displacements

might also have been influenced by the excavation activities that were taking place in the area: the mine staff reported that acceleration of the slope was mostly observed as material was removed, whereas deceleration occurred when mining was stopped. Still, regardless of the cause, and although requiring additional data smoothing, it was possible to extrapolate tertiary creep behavior in the precursor displacements of failure #5.

4.4. “Signature” of the failure events

The analysis of the dataset also highlighted specific parameters that may be used to differentiate failures and non-failures. In Fig. 11 the plot of peak velocity vs. peak acceleration for the 9 instabilities is reported, indicating that failures #1–#4 were anticipated by significantly larger values of these parameters. Even non-failure #3, which featured highly alarming values of peak velocity and acceleration during a phase of apparent tertiary creep (25.3 mm/h and 14.9 mm/h², respectively), is at a significant distance from the area of the graph where failures

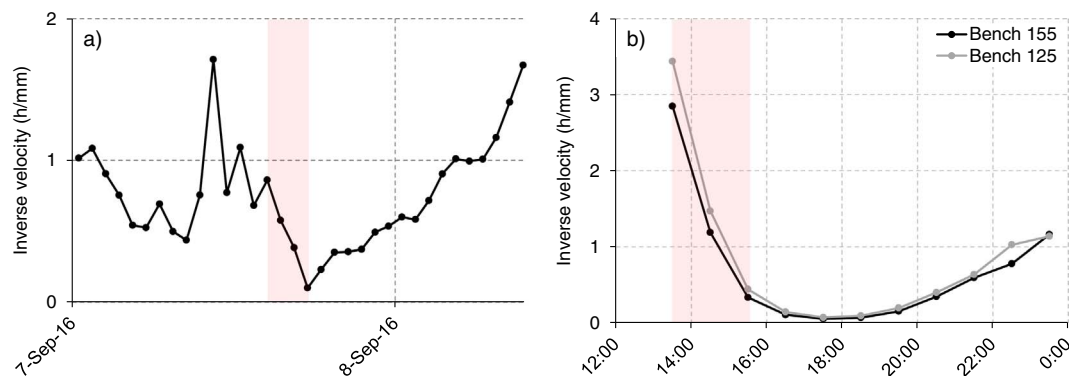


Fig. 10. Inverse velocity plots of failures (a) #1 and (b) #3 (19 June 2008). The red shaded areas include the plot sections that, in a scenario of near real-time monitoring, could be considered for failure-time prediction. (For interpretation of the references to color in this figure legend, the reader is referred to the web version of this article.)

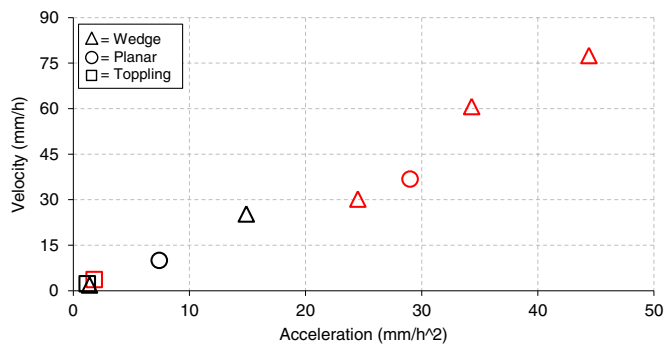


Fig. 11. Plot of peak velocity vs. peak acceleration. Red markers represent failures, black markers non-failures. (For interpretation of the references to color in this figure legend, the reader is referred to the web version of this article.)

#1–#4 are located. A threshold separating the two groups may be preliminarily defined around values of 30 mm/h and 20 mm/h². The two toppling instabilities are both identified in the lower left part of the graph; this may be associated with the different characteristics of their deformation behavior, as previously described. Even so, it is worth noting that the toppling failure was anticipated by greater peak velocity and acceleration with respect to the toppling non-failure. This introduces a possible additional level of discrimination for the phase of early warning, as it may be convenient to define specific alarm thresholds on the basis of the failure mechanism.

Similarly, another parameter to be evaluated is the scale of the instabilities. Fig. 12 shows the same peak velocity vs. peak acceleration plot of Fig. 11, with the size of the markers being proportional to the estimated mass of the respective instability. The estimated masses of failures #1–#4 were relatively limited (approximately 1500 to 4000 t, Table 2), whereas the non-failures were considerably larger (approximately 35,000 to 750,000 t excluding the toppling non-failure #2, Table 3). The scales of the two cases of toppling (dashed markers in Fig. 12) were instead basically equivalent (approximately 10,000 and 7500 t). The aforementioned discrepancy may be explained as follows: while small instabilities (such as failures #1–#4) can be associated to a single rock block moving on a predefined discontinuity (or pair of discontinuities in the case of wedge failures), on the other hand large instabilities are likely to consist of several interacting blocks moving and rotating reciprocally in correspondence of a number of different surfaces, thus allowing the slope to accommodate large values of total displacement and velocity without necessarily involving an evolution towards critical stability. This is in agreement with the prolonged and intense phases of deformation that were observed especially in non-failures #1 and #3; for these slopes to fail, larger rates of movement

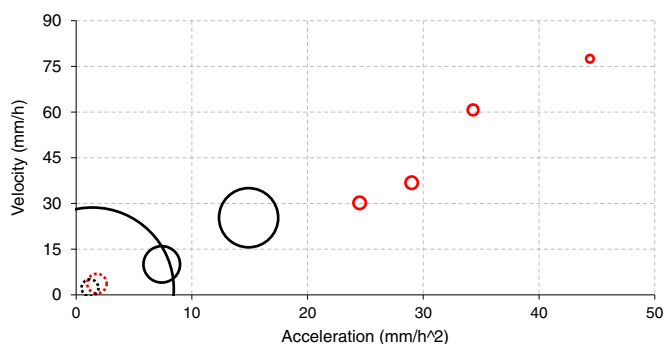


Fig. 12. Plot of peak velocity vs. peak acceleration, with the size of the markers being proportional to the estimated mass (t) of the instabilities (see Tables 2 and 3). Red circles represent failures, black circles non-failures. The dotted circles indicate toppling instabilities. (For interpretation of the references to color in this figure legend, the reader is referred to the web version of this article.)

may be deemed necessary as precursors.

4.5. Recommendations on alarming procedures for brittle failures and predictability

The setup of a slope monitoring program in a context of markedly brittle slope failures, such as that of the considered open-pit case study, presents several challenges. Procedures of data acquisition and analysis should thus be carefully calibrated. Owing to the sudden nature and the potential rapidity of the accelerations, it is of crucial importance that slope monitoring of hard rock masses is performed at a very high frequency of acquisition, in the range of one measurement every few minutes (e.g. 5 min or less). The open-pit data showed that a 20-min frequency of acquisition was in fact barely acceptable or, in the case of failure #1, inadequate. Such observations have repercussions also on the length of the time window over which data need to be smoothed. Since to a wider time window corresponds more lag introduced to the identification of trend changes, it follows that measurements should be averaged over an interval of 1 h or less, even if at the cost of increased noise in the time series.

In terms of failure predictability, the tertiary creep theory showed to be theoretically applicable even to brittle slope failures in hard rock masses. However, the failure-time extrapolation from inverse velocity plots depends on a proper assessment of the trend towards the horizontal axis, which can be carried out given the availability of a sufficient number of data points included in such trend (Dick et al., 2015; Carlà et al., 2016). This further limits how much in advance the imminence of a failure can be determined, as well as the time for undertaking the necessary response actions and evacuation procedures. The fact that tertiary creep, even if featuring considerable velocities, may not always anticipate failure (Fig. 10; also discussed in Fell et al., 2000, and Hutchinson, 2001), adds uncertainty to the setup of an early warning system aimed at reducing as much as possible the number of false alarms.

At the same time, Figs. 11 and 12 suggest that the implementation of alarms based on thresholds of velocity and/or acceleration is appropriate. Failures #1–#4 were in fact associated with distinctly larger values of these two parameters. Moreover, different thresholds may be established on the basis of the mechanism and/or size of the instability. Increasing confidence may be obtained in the future as more case studies are acquired and these plots are further populated.

It is worth noting that all the considerations above are based on a data analysis conducted in retrospect. The additional constraints and problematics that are inherent to near real-time slope monitoring in open-pit mines should therefore be taken into account. An alarming system consisting of a sequence of thresholds representative of increasing risk scenarios may be defined as follows:

- I. Threshold Level 1: corresponding to a value of velocity slightly above the noise level of the radar and associated to LOS measurements (e.g. 1–2 mm/h). It identifies the initial stage of emergency management. This is a conservative threshold to be used in case the direction of slope movement, and thus the radar sensitivity, are not yet known.
- II. Threshold Level 2: based on a larger value of velocity, to be established over moving areas where Threshold Level 1 was exceeded, and following calculation of the radar sensitivity. This threshold refers to corrected radar measurements, and may be further increased after evaluation of mechanism and size of the instability.
- III. Threshold Level 3: combining both velocity and acceleration, and determined as the separation between failures and non-failures in a peak velocity vs. peak acceleration plot derived from past case studies at the site (e.g. 30 mm/h and 20 mm/h² in Fig. 11). Failure-time predictions should be continuously performed once the movement rate of the slope approaches this last threshold level.

Finally, it can be evinced that the mitigation of slope failure risk is not to be performed according to a black box approach, i.e. by acquiring and analyzing data without any knowledge on the specific issues related to the monitored scenario. The latter observation applies to both open-pit mine operations and natural slopes. In particular, the setup of effective monitoring programs and early warning systems is strictly dependent on their appropriate calibration and contextualization in the frame of the on-site characteristics and deformation behavior. While to this point the geomechanical properties of the rock mass can give a general indication, the back-analysis of monitoring data from past slope instabilities (assuming their availability) is of crucial importance. Since the nature of the slope deformation may also vary depending on several other factors, as many complementary data as possible need to be collected and reviewed.

5. Conclusions

The mitigation of slope failure risk is an essential part of the safety strategies in open-pit mines. Studying the typical slope deformation behavior in the pit is crucial to the setup of monitoring programs and early warning systems, and in this sense considerable insight may be gained by reviewing monitoring data relative to past cases of instability.

The analysis of radar monitoring data from 9 cases of instability at an undisclosed open-pit mine provided the opportunity to analyze in detail the deformation of hard rock masses subject to markedly brittle failure. The goal of such an analysis was to define the characteristics of the slope movements in the pit and the appropriate strategy for the setup of alarms. This also allowed to assess whether, as opposed to the common perception, it is possible to effectively predict and manage brittle slope failures by evaluating the trend of the precursor deformation. Adding to this topic, another point of interest was to separately characterize the failures from the cases of instability that, although showing considerable displacements, ultimately did not evolve into failure (“non-failures”), and consequently to define a sort of “signature” of the failure events.

The results showed that tertiary creep indeed affects also rock slopes of high geomechanical quality, and that it may develop very rapidly on a scale of a few hours. This has obvious repercussions in terms of frequency of measurement acquisition and reference interval of the data processing that are needed in order to successfully predict failures and provide sufficient notice for the necessary response actions and evacuation procedures. The case studies were also considered in terms of peak velocity and acceleration, following which it was determined that the failures were anticipated by significantly larger values of these two parameters.

It was observed that other factors possibly influencing the slope deformation behavior and tendency to failure are the size and mechanism of the instability. In particular, failures #1–#4 were all of relatively small size (estimated mass of 4000 t or less), whereas non-failures were typically 1 or more order of magnitudes larger. In a context of near real-time slope monitoring, it is then essential to take in due consideration also these (and possibly other) parameters, as it may be convenient to set different alarm thresholds depending on geometry and properties of the detected slope movement. Strictly related to all the above is the importance to account for the variable radar LOS sensitivity across the pit, as uncorrected measurements of displacement may point to highly misleading observations and to a false perception of the inherent risk.

It is concluded that any slope monitoring program and early warning system is effective only if calibrated and contextualized in the frame of the on-site slope characteristics and deformation behavior. Such consideration is deemed to be valid for the mitigation of slope failure risk in both artificial and natural slopes.

References

- Antonello, G., Casagli, N., Farina, P., Leva, D., Nico, G., Sieber, A.J., Tarchi, D., 2004. Ground-based SAR interferometry for monitoring mass movements. *Landslides* 1 (1), 21–28.
- Armstrong, J., Rose, N.D., 2009. Mine operation and management of progressive slope deformation on the south wall of the Barrick Goldstrike Betze-Post Open Pit. In: *Proceedings of Slope Stability 2009: International Symposium on Rock Slope Stability in Open Pit Mining and Civil Engineering*, Santiago.
- Atzeni, C., Barla, M., Pieraccini, M., Antolini, F., 2015. Early warning monitoring of natural and engineered slopes with ground-based synthetic-aperture radar. *Rock Mech. Rock. Eng.* 48 (1), 235–246.
- Bardi, F., Raspini, F., Frodella, W., Lombardi, L., Nocentini, M., Gigli, G., Morelli, S., Corsini, A., Casagli, N., 2017. Monitoring the rapid-moving reactivation of earth flows by means of GB-InSAR: the April 2013 Capriglio landslide (Northern Apennines, Italy). *Remote Sens.* 9 (2), 165.
- Carlà, T., Intrieri, E., Di Traglia, F., Nolesini, T., Gigli, G., Casagli, N., 2016. Guidelines on the use of inverse velocity method as a tool for setting alarm thresholds and forecasting landslides and structure collapses. *Landslides* in press. <http://dx.doi.org/10.1007/s10346-016-0731-5>.
- Casagli, N., Catani, F., Del Ventisette, C., Luzi, G., 2010. Monitoring, prediction, and early warning using ground-based radar interferometry. *Landslides* 7 (3), 291–301.
- Casagli, N., Frodella, W., Morelli, S., Tofani, V., Ciampalini, A., Intrieri, E., Raspini, F., Rossi, G., Tanteri, L., Lu, P., 2017. Spaceborne, UAV and ground-based remote sensing techniques for landslide mapping, monitoring and early warning. *Geoenviron. Disaster* 4 (9), 1–23.
- Crosta, G.B., Agliardi, F., 2002. How to obtain alert velocity thresholds for large rock-slides. *Phys. Chem. Earth* 27, 1557–1565.
- Di Traglia, F., Nolesini, T., Intrieri, E., Mugnai, F., Leva, D., Rosi, M., Casagli, N., 2014. Review of ten years of volcano deformations recorded by the ground-based InSAR monitoring system at Stromboli volcano: a tool to mitigate volcano flank dynamics and intense volcanic activity. *Earth-Sci. Rev.* 139, 317–335.
- Dick, G.J., Eberhardt, E., Cabrejo-Liévano, A.G., Stead, D., Rose, N.D., 2015. Development of an early-warning time-of-failure analysis methodology for open-pit mine slopes utilizing ground-based slope stability radar monitoring data. *Can. Geotech. J.* 52 (4), 515–529.
- Doyle, J.B., Reese, J.D., 2011. Slope monitoring and back analysis of east fault failure, Bingham Canyon Mine, Utah. In: *Proceedings of Slope Stability 2011: International Symposium on Rock Slope Stability in Open Pit Mining and Civil Engineering*. Canadian Rock Mechanics Association, Vancouver, BC.
- Eberhardt, E., Stead, D., Coggan, J.S., 2004. Numerical analysis of initiation and progressive failure in natural slopes – the 1991 Randa rockslide. *Int. J. Rock Mech. Min. Sci.* 41, 69–87.
- Fanti, R., Gigli, G., Lombardi, L., Tapete, D., Canuti, P., 2013. Terrestrial laser scanning for rockfall stability analysis in the cultural heritage site of Pitigliano (Italy). *Landslides* 10 (4), 409–420.
- Farina, P., Coli, N., Yön, R., Eken, G., Keitzmen, H., 2013. Efficient real time stability monitoring of mine walls: the Çöllolar Mine Case Study. In: *Proceedings of the 23rd International Mining Congress & Exhibition of Turkey*, Antalya, Turkey, pp. 111–117.
- Farina, P., Coli, N., Coppi, F., Babboni, F., Leoni, L., Marques, T., Costa, F., 2014. Recent advances in slope monitoring radar for open-pit mines. In: *Proceedings of Mine Closure Solutions 2014*, Ouro Preto, Minas Gerais, Brazil, (ISBN: 978-0-9917905-4-8).
- Federico, A., Popescu, M., Elia, G., Fidelibus, C., Internò, G., Murianni, A., 2012. Prediction of time to slope failure: a general framework. *Environ. Earth Sci.* 66, 245–256.
- Fell, R., Hung, O., Leroueil, S., Riemer, W., 2000. Geotechnical engineering of the stability of natural slopes and cuts and fills in soil. In: *Proceedings of the International Conference on Geotechnical and Geological Engineering*, Melbourne, pp. 21–120.
- Fukuzono, T., 1985. A new method for predicting the failure time of a slope. In: *Proceedings of the 4th International Conference and Field Workshop on Landslides*, Tokyo, pp. 145–150.
- Gigli, G., Frodella, W., Mugnai, F., Tapete, D., Cigna, F., Fanti, R., Intrieri, E., Lombardi, L., 2012. Instability mechanisms affecting cultural heritage sites in the Maltese archipelago. *Nat. Hazards Earth Syst. Sci.* 12, 1883–1903.
- Gigli, G., Morelli, S., Fornera, S., Casagli, N., 2014. Terrestrial laser scanner and geomechanical surveys for the rapid evaluation of rock fall susceptibility scenarios. *Landslides* 11 (1), 1–14.
- Ginting, A., Stawski, M., Widiadi, R., 2011. Geotechnical risk management and mitigation at Grasberg Open Pit, PT Freeport Indonesia. In: *Proceedings of Slope Stability 2011: International Symposium on Rock Slope Stability in Open Pit Mining and Civil Engineering*, Canadian Rock Mechanics Association, Vancouver, BC.
- Gokceoglu, C., Sonmez, H., Ercanoglu, M., 2000. Discontinuity controlled probabilistic slope failure risk maps of the Altindag (settlement) region in Turkey. *Eng. Geol.* 55, 277–296.
- Hutchinson, J., 2001. Landslide risk – to know, to foresee, to prevent. *Geologia Technica Ambientale* 9, 3–24.
- Intrieri, E., Gigli, G., 2016. Landslide forecasting and factors influencing predictability. *Nat. Hazards Earth Syst. Sci.* 75 (24), 2501–2510.
- Intrieri, E., Gigli, G., Casagli, N., Nadim, F., 2013. Brief communication “landslide early warning system: toolbox and general concepts”. *Nat. Hazards Earth Syst. Sci.* 13, 85–90.
- Lacasse, S., Nadim, F., 2009. Landslide risk assessment and mitigation strategy. In: *Landslides – disaster risk reduction*. Springer, Berlin Heidelberg, pp. 31–61.
- Luzi, G., Pieraccini, M., Mecatti, D., Noferini, L., Macaluso, G., Galgaro, A., Atzeni, C.,

2006. Advances in ground based microwave interferometry for landslide survey: a case study. *Int. J. Remote Sens.* 27 (12), 2331–2350.
- Macciotta, R., Hendry, M., Martin, C.D., 2016. Developing an early warning system for a very slow landslide based on displacement monitoring. *Nat. Hazards* 81 (2), 887–907.
- Macqueen, G.K., Salas, E.I., Hutchison, B.J., 2013. Application of radar monitoring at Savage River Mine, Tasmania. In: *Proceedings of Slope Stability 2013: International Symposium on Rock Slope Stability in Open Pit Mining and Civil Engineering*, Australian Centre for Geomechanics, Brisbane, Australia.
- Monserrat, O., Crosetto, M., Luzzi, G., 2014. A review of ground-based SAR interferometry for deformation measurement. *ISPRS J. Photogramm. Remote Sens.* 93, 40–48.
- Morales, M., Panthi, K., Botsialas, K., Holmøy, K.H., 2017. Development of a 3D structural model of a mine by consolidating different data sources. *Bull. Eng. Geol. Environ.* <http://dx.doi.org/10.1007/s10064-017-1068-6>.
- Paronuzzi, P., Bolla, A., Rigo, E., 2016. Brittle and ductile behavior in deep-seated landslides: learning from the Vajont experience. *Rock Mech. Rock. Eng.* 49, 2389–2411.
- Read, J., Stacey, P., 2009. *Guidelines for Open Pit Slope Design*. CSIRO Publishing, Australia.
- Rose, N.D., Hungr, O., 2007. Forecasting potential rock slope failure in open pit mines using the inverse-velocity method. *Int. J. Rock Mech. Min. Sci.* 44, 308–320.
- Vaziri, A., Moore, L., Ali, H., 2010. Monitoring systems for warning impending failures in slopes and open pit mines. *Nat. Hazards* 55 (2), 501–512.
- Voight, B., 1988. A method for prediction of volcanic eruptions. *Nature* 332, 125–130.
- Voight, B., 1989. A relation to describe rate-dependent material failure. *Science* 243, 200–203.
- Zavodni, Z.M., Broadbent, C.D., 1980. Slope failure kinematics. *Bull. Can. Inst. Min.* 73 (816), 69–74.